

Tunneling magnetoresistance in Mn_2Au -based pure antiferromagnetic tunnel junction

Xingtao Jia,^{1,*} Hui-Min Tang,^{2,†} and Shi-Zhuo Wang³

¹*School of Physics and Electronic Information Engineering,
Henan Polytechnic University, Jiaozuo 454000, China*

²*School of Physical Science and Technology, Guangxi Normal University, Guilin 541001, China.*

³*School of Physics and Electronic Engineering, Zhengzhou University of Light Industry, Zhengzhou 450002, China*
(Dated: March 21, 2023)

Antiferromagnetic (AF) spintronics is merit on ultra-high operator speed and stability in the presence of magnetic field. To fully use the merit, the device should be pure rather than hybrid with ferromagnet or ferrimagnet. For the magnetism in the antiferromagnet is canceled by that of different sublattices, breaking the symmetry in the material can revive the native magnetism, which can be detected by the magnetoresistance (MR) effect. Achieving noticeable MR effect in the pure AF device is difficult but essential for the AF spintronic applications. Here, we study the tunnel magnetoresistance (TMR) effect in the $\text{Nb}/\text{Mn}_2\text{Au}/\text{CdO}/\text{Mn}_2\text{Au}/\text{Nb}$ pure AF magnetic tunnel junctions (AF-MTJs) based on a first-principle scattering theory. Giant TMRs with order of 1000% are predicted in some symmetric junctions, which is originated from the interfacial resonance tunneling effect related with the k_{\parallel} dependent complex band structures of CdO and Mn_2Au in companion with the enhanced spin polarization of the interfacial magnetic atoms. The effect of voltage bias and interfacial disorder such as Oxygen vacancy, Manganese vacancy, and Manganese-Cadmium exchanges at $\text{Mn}_2\text{Au}/\text{CdO}$ interfaces are studied also. Our studies suggest $\text{Nb}/\text{Mn}_2\text{Au}/\text{CdO}/\text{Mn}_2\text{Au}/\text{Nb}$ AF-MTJs promising material for AF spintronic application, and rocksalt CdO a potential symmetry filtering material for spintronic applications.

I. INTRODUCTION

As one candidate of the next generation electronics, antiferromagnetic (AF) spintronics is merit on ultra-high speed spin dynamics up to THz and insensitivity to magnetic field,[1, 2] which is promising as the magnetic memories and magnetic sensors, and also demonstrates potential application for brain-inspired computation. To fully use the merit, the AF spintronic devices should avoid to use ferromagnet (FM) and ferrimagnet as reference layer or pinning layer. That is, which should be pure rather than hybrid. Magnetoresistance (MR) effect is general in the magnet. The no-relativistic MR effect is always larger than the relativistic one. The MR effect in the pure AF spin valves (AF-SVs) is different in principle from that in the ferromagnetic one,[3] which is small in general and hard to meet the commercial demand. By taking advantage of the perfect spin filter effect of the MgO barrier, tunneling MR (TMR) effect over several hundreds percent can be found in some hybrid AF tunnel junctions(AF-MTJs) with FM as spin polarizer and antiferromagnet (AFM) as active layer. [4, 5] Recent studies predict giant TMR up to several thousand percent in the sandwich-type van der Waals (vdW) magnetic tunnel junctions,[6–10] which is related with the magnetic state dependent band structure. Unconventional colossal angular MRs are found in the semiconductor-type AFM EuTe_2 with space-time inversion symmetry-broken[11], where the metal-insulator transition (MIT) induced by

the magnetic field should be responsible for. Large TMR as high as 300% are predicted first-principally in the Mn_3Sn based AF-MTJs originated from the spin-splitting in the moment space[12], and TMR about 100% in RuO_2 based AF-MTJ originated from spin-momentum coupling[13].

Electric current is preferred to manipulate the AFM,[1, 2, 14, 15] which is compatible to the state-of-art semiconductor technology. When the current flows through the AF metal with broken inversion symmetry, the Néel spin-orbit torque (NSOT)[16–19] and spin orbital torque (SOT)[20] can manipulate the Néel order with a current density around 10^6 A/cm^2 , which is comparable to the current induced spin transfer torque (STT) in the well-studied MgO -based ferromagnetic tunnel junctions (F-MTJs).[21–23] Current flowing through the noble metal can induce spin Hall effect (SHE), which can be used to manipulate the Néel vector of AFM.[24] Antidamping torque from the SHE effect can be used to control the Néel order efficiently by control the epitaxial orientation.[25] Generally, the switching current in AFM using SHE is orders in magnitude larger than that using NSOT effect for the lower efficiency of the former, which can be considerable enhanced by topological surface states.[26]

The spin dynamics in the AFM can be depicted by a coupled Landau-Lifshitz-Gilbert (LLG) equation.[1, 2] Therein, the time scale of the spin dynamics is dependent on the exchange field between the magnetic moments. The spin dynamics in the synthetic 2D AFM is more similar to that in the spin valve with two FMs sandwiched by non-magnetic materials. The synthetic 2D AFM can show giant MR effect,[6–10] but cannot be considered as AF spintronic device. To fully realize the merits of the

*Corresponding author, E-mail:jiaxingtao@hpu.edu.cn

†Corresponding author, E-mail:hmtang@gxnu.edu.cn

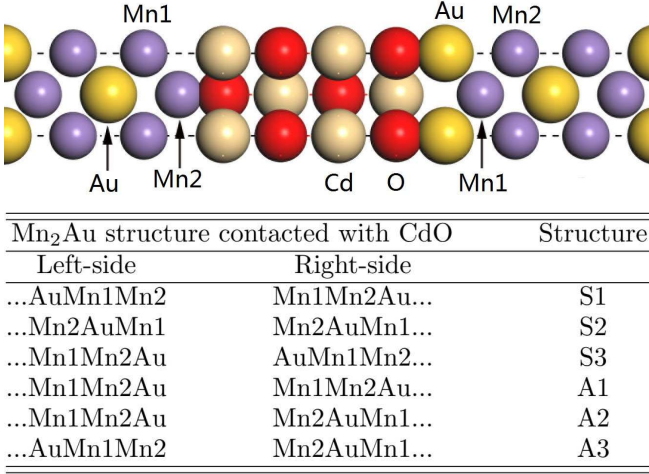


FIG. 1: Schematic Mn₂Au/CdO/Mn₂Au(001) multilayer used in the study. Therein, Mn₂Au follows a ...ABCABC... structure along the [001] direction with A, B and C standing for Au, Mn at site one (Mn1), and Mn at site two (Mn2), respectively. According to the termination atoms of Mn₂Au contacted with CdO, we define three symmetric structures named as S1, S2 and S3 and three asymmetric structures named as A1, A2 and A3.

AFM, all the magnetic materials in the AF spintronic device should be intrinsic AFM. Unfortunately, reports about the MR effect in the pure AF spintronic device is rare. Seeking a pure AF device with large MR effects and good accommodation with the current-in-art semiconductor architecture is necessary and urgent for the AF spintronic applications.

Sizeable MR effect in the hybrid AF spintronic device is believed to be related with the localized interfacial states,[5, 24] which demand that the interfaces should be as clean as possible. The interfacial disorders, including the atomic disorder and spin disorder, can destroy the interfacial states, which is key factor for sizeable MR effect in the hybrid AF-MTJs.[4, 5] To realize ideal interfaces, epitaxial contact between the AF metal and non-magnetic insulator should be favorable. Here, we focus on epitaxial Mn₂Au/CdO/Mn₂Au pure AF-MTJs with ideal interface. Tetragonal Mn₂Au shows high Néel temperature above 1000K.[27] Current induced NSOT effect is efficient to manipulate the Néel vector of metallic Mn₂Au for the broken inversion symmetry structure.[16] Cubic CdO shows rocksalt (NaCl) structure with lattice parameter $a = 4.69$ Å, which can match well with the tetragonal Mn₂Au by rotation of 45 degree. For the current induced STT is inefficiency to manipulate the Néel order of the AFM in the perpendicular magnetic structure, three terminals structure using NSOT or SHE effect is more favorable. In these case, the Mn₂Au layer thickness should be as thinner as possible. Bcc Nb or Ta with lattice parameter $a = 3.3$ Å can be used as leads, which can match well with Mn₂Au also, and the former is more favorable for low price.

II. METHODS

A two-terminal structure with Mn₂Au/CdO/Mn₂Au sandwiched between two semi-infinite Nb leads was used to study the MR effect in the study. The stacking of Mn₂Au/CdO/Mn₂Au multilayer is shown in Fig. 1. We firstly carry Density functional theory (DFT) calculations based on the plane wave function to found the stable structure, and then carry tight-binding linear muffin-tin orbital (TB-LMTO) calculations to get the potentials of the system, and finally transfer the potentials into a Wave-Function-Matching (WFM) package to calculate the spin transports.

A. Structure calculations

We use DFT calculations based on the projector augmented wave (PAW) potential and PBE exchange-correlation function[28] to find stable structures. A slab structure containing 6 Ls CdO and 6 Ls Mn₂Au is used to study the Mn₂Au/CdO(001) interface. During calculations, we expand CdO to match with Mn₂Au, and all parameters are fixed to their bulk state and the only free parameters is the distance between Mn₂Au and CdO. A cutoff energy of 600 eV is taken for all calculations. DFT calculations indicate the O termination (of CdO) cases are energy stable. The total energies are -129.092, -130.038, and -130.047 eV for the Au, Mn1, and Mn2 atoms (of Mn₂Au) bonding with O atoms (of CdO) with bonding lengths around 2.41, 2.03 and 1.93 Å, and we denote the structures as "Au termination", "Mn1 termination" and "Mn2 termination" in the study, respectively. That is, the Mn₂Au/CdO interface with Mn2 termination structure most energy favorable. For the Nb/Mn₂Au interface, the DFT calculations indicate that the structure with Mn2 atoms (of the Mn₂Au layer) sited above the second monolayer Nb atoms (of the Nb layer) is more energy favorable.

B. potential calculations

The potentials used in the transport package are obtained via self-consistent calculations performed using TB-LMTO surface Green's function method with a coherent potential approximation (CPA) to deal with imperfections.[29] For Nb, the atomic sphere has radius 1.639 Å whose space fills the bcc lattice. For Mn₂Au, same atomic radius of 1.555 Å are used for both Au and Mn atoms to fill the tetragonal lattice. Inside CdO, we take radius 1.492 Å for oxygen atoms and 1.237 Å for Cd atoms, and vacuum sphere of radius 0.796 Å is added at the center of the cube with 4 O atoms and 4 Cd atoms to fill the space. The direct band gap of CdO present at Γ point is around 2.85 eV using modified Becke-Johnson (mBJ)[30] potential within local spin density approximation (LDA), and the conduction band minimum (CBM) is

around 1.3 eV above the Fermi energy. Indirect band gap is around 1.5 eV with the valance band maximum (VBM) localized at L point (see Fig.3B). The band structure is consistent with the experimentals[31, 32]. Three empty spheres are introduced to fill the $\text{Mn}_2\text{Au}/\text{CdO}$ interface during the self-consistent and spin transport calculations. Therein, two vacuum spheres with radius r_1 are inserted exactly above the vacuum spheres inside the CdO, and a vacuum sphere with radius r_2 is added exactly above the Cd atom. The former are considered to belong to the CdO layer, and the positions of the latter is arranged to minimize overlap. For the Mn2 termination structure, both r_1 and r_2 are set to 0.653 Å. For the Mn1 termination structure, both r_1 and r_2 are set to 0.796 Å and 0.668 Å, respectively. For the Au termination structure, both r_1 and r_2 are set to 0.796 Å and 0.956 Å, respectively.

C. transport calculations

The spin transport calculations were carried out via a first-principle WFM method[33] for the ideal junctions. For cases with interfacial disorders, the vertex correction[34] is used to average the configurations. The Néel order vectors of Mn_2Au are defined by the direction of the magnetic moments of the first Mn atom contacted with CdO. The left-side Néel order was fixed as reference, and the right-side Néel order set free. A 1600×1600 k -mesh for most structures was used to sample the 2D Brillouin zone (BZ) to ensure good numerical convergence for the ideal epitaxial structures.

III. RESULTS AND DISCUSSION

The first-principle density-functional theory (DFT) calculations indicate that the $\text{Mn}_2\text{Au}/\text{CdO}$ interface with O atoms (of CdO) bonding with Mn2 atoms (of Mn_2Au) is most energy stable. We denote the structure as "Mn2 termination", and pay more attention to the structure in the study. Comparatively, metastable interfaces with O atoms bonding with Au and Mn1 atoms are considered less. According to the types of $\text{Mn}_2\text{Au}/\text{CdO}$ interface, there are six structures in the $\text{Mn}_2\text{Au}/\text{CdO}/\text{Mn}_2\text{Au}$ multilayer, as shown in Fig. 1. Therein, the S1 structure is more energy favorable, and we focus on the structure in the study. The tetragonal Mn_2Au shows fourth-order in-plane anisotropy with hard axis along z direction and easy axis along $\theta = 90^\circ$, $\phi = \pm 45^\circ$, and $\pm 135^\circ$. [35] According to the relative angle Θ between the Néel vector of the reference (left) side (n_L) and the free (right) side (n_R), there are three stable magnetic states labeled as the parallel (P), perpendicular (PP), and antiparallel (AP) states, corresponding to $\Theta = 0, \pi/2$, and π , respectively. We define the angular-dependant TMR as $\text{TMR}(\Theta) = R(\Theta)/R(0) - 1$ with resistance $R = 1/G$ with

conductance $G = (e^2/h)\text{Tr}(tt^\dagger)$, where t is the transmission part of the scatter matrix S .

A. TMRs in the AF-MTJs

Firstly, we take a look at the thickness dependency of the TMRs. Figure 2A and B give the spin transmissions and TMRs in the ideal $\text{Nb}/\text{Mn}_2\text{Au}(12-120)/\text{CdO}(4-20)/\text{Mn}_2\text{Au}(12-120)/\text{Nb}$ pure AF-MTJs with S1 structure, where the numbers in the bracket indicate the thickness in atomic layers (Ls). We name these junctions using Nb leads as "Nb lead" junctions. Firstly, we vary the thickness of Mn_2Au while fix 10 Ls CdO as shown in Fig. 2A. Therein, the spin transmissions of the AP structure are less sensitive to the thickness of the Mn_2Au region, but about one order in magnitude smaller than that of the very very thicker Mn_2Au junction, which can be considered as using Mn_2Au as leads and we name it as " Mn_2Au lead" junction. The spin transmissions of the AF-MTJs with P and PP magnetic states increase firstly and then decrease with peak values present around 18 Ls Mn_2Au , with the peak values around threefold larger than that of the junction with 120 Ls Mn_2Au , and around one order in magnitude larger than that of the " Mn_2Au lead" junction. Considering the metallicity of tetragonal Mn_2Au , [4] the huge sensitivity of the spin transmission in the AF-MTJs with respect to the Mn_2Au thickness is unusual. The TMR studies indicate giant TMRs with range from 1600% to 5600% in the AF-MTJs as Mn_2Au vary from 12 to 120 Ls, which is about one order in magnitude larger than that of the " Mn_2Au lead" junction, as shown in the inset of Fig. 2A. The TMRs in these junctions are comparable to the specular TMR effect found in the well-studied MgO-based F-MTJs. [21, 22, 36, 37] Moreover, the spin transmission of the AF-MTJs follows the simple trigonometric functions, and the TMR effect of the PP magnetic states are around 50% of that of the P states.

The spin transmissions in both the "Nb lead" and " Mn_2Au lead" AF-MTJs decrease exponentially as the CdO thickness increases, with considerable deviation in that with P and PP magnetic states when the barriers are thinner, as shown in Fig. 2B. Here, we fix 24 Ls Mn_2Au for the "Nb lead" junctions during the calculations. As the CdO thickness increases, the TMRs of both types junctions increase quickly initially, and then slow down, and finally decrease slowly with peak around 14 Ls CdO. For the junctions with P magnetic state, the least and largest TMRs are 270% (in junction with 4 Ls CdO) and 13000% for the "Nb lead" junctions, which are 105% and 920% for the " Mn_2Au lead" junctions. When the CdO is thicker, the TMRs of the "Nb lead" junctions is about one order in magnitude larger than that of the " Mn_2Au lead" junctions. The giant difference indicates the presence of spin filtering effect in the "Nb lead" junctions.

Following to the two-current model, the current flows

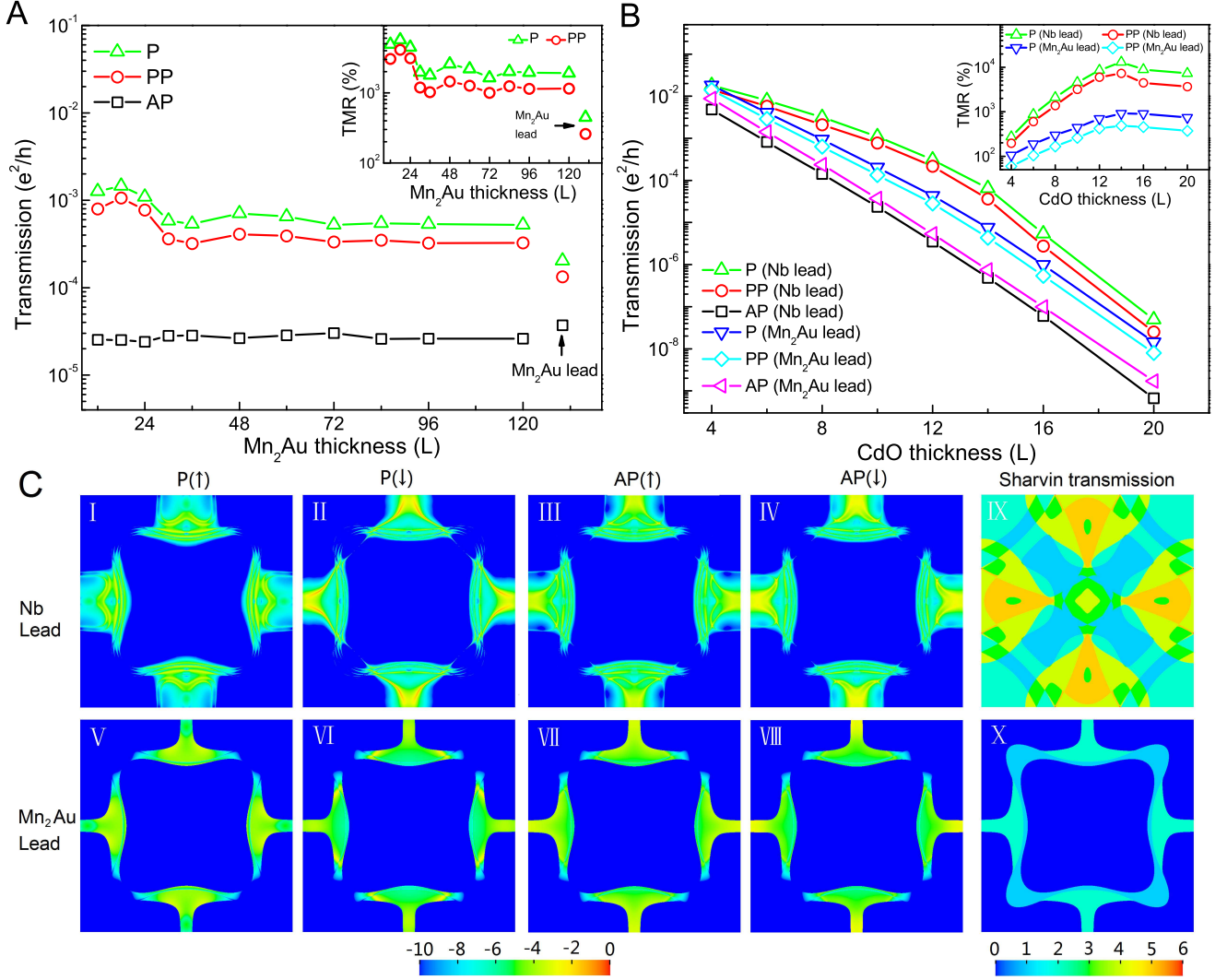


FIG. 2: (A) Mn_2Au thickness dependency and (B) barrier thickness dependency of the spin transmissions and TMRs of the ideal Nb/ Mn_2Au /CdO/ Mn_2Au /Nb and Mn_2Au /CdO/ Mn_2Au pure AF-MTJs with S1 structure. The CdO barrier thickness is set 10 Ls in (a), and both the reference and free Mn_2Au layers are set 24 Ls in (b) for the "Nb lead" junctions. (C) $k_{||}$ resolved transmission coefficient in the 2D BZ of the ideal (I-IV) Nb/ Mn_2Au (24)/CdO(10)/ Mn_2Au (24)/Nb(001) and (V-VIII) Mn_2Au /CdO(10)/ Mn_2Au (001) pure AF-MTJs with S1 structure at Fermi energy, and Sharvin transmission of (IX) bcc Nb and (X) tetragonal Mn_2Au along the [001] direction.

through the barrier should be spin polarized to induce MR effect. In the limit of non-relativistic case, the current flowing through the AF metal Mn_2Au is hard to spin-polarize. However, the spin transmissions and TMRs calculations above indicate that the Mn_2Au layers are almost half-metallic, which maybe relate with the interface effect as found in the Fe/MgO/Ag/ Mn_2Au [4] hybrid AF-MTJs.

Figure 2C(I-IV) gives the $k_{||}$ resolved spin transmission of the ideal Nb/ Mn_2Au (24)/CdO(10)/ Mn_2Au (24)/Nb AF-MTJs with S1 structure at the Fermi energy. For the P (AP) magnetic state of the "Nb lead" junctions, the sum of the $k_{||}$ resolved spin transmission of the majority (\uparrow) and minority (\downarrow) spin is $5.75(0.116) \times 10^{-4} e^2/h$

and $2.29(0.117) \times 10^{-4} e^2/h$, respectively. That is, the both spin channels contribute almost equally to the spin transmission of the P magnetic states. This is noticeably different from that in the F-MTJs with considerable MR effect, where the spin transmission is spin polarized.[21] Looking at the 2D Brillouin zone (BZ)(Fig. 2C(I) and (II)), it clearly that the hot spots and hot lines dominate the total transmission for both spin channels, and they are highly spin polarized and locate in different regions. The sum of resonant $k_{||}$ points with transmission possibility larger than 0.01 contribute to about 94% and 40% of the total spin transmission of the P and AP magnetic state of the "Nb lead" junction. About one-fourth of the 2D BZ contributes to the Sharvin conductance

of bulk Mn_2Au at the Fermi energy, as shown in Fig. 2C(X), and we name the region as Sharvin area, which can be understood by the projection of Fermi surface (Fig. 3D(I)) along the [001] direction and indicate Mn_2Au a $k_{||}$ resolved barrier materials. The $k_{||}$ points out of the Sharvin area of Mn_2Au contribute to about 67% and 7% of the total transmission for the \uparrow and \downarrow spin of the P magnetic state, respectively. It is less than 1% for both spin channels for the AP state. The resonance $k_{||}$ points within and out of the Sharvin area of Mn_2Au show difference in details. Both the bonding and antibonding peaks (with energy gap around 10^{-1}eV) of the former are splitting further into two peaks with energy gap around 10^{-4}eV . This maybe related with the complex coupling of the interfacial states.

The $k_{||}$ resolved spin transmission in the "Mn₂Au lead" junctions is given in Fig. 2C(V-VIII). Similar to the "Nb lead" junctions, the bright areas of the \uparrow and \downarrow spin channels of the P magnetic state of the junction are located in different regions of the 2D BZ also, and the spin transmission is not only spin dependent but also $k_{||}$ dependent. The sum of spin transmission give a larger spin polarization of 9% compared with that in the "Nb lead" junction.

B. Band structure of the system

Núñez et al.,[3] gives a theoretical model to estimate the MR effect in the L-type AFM with MR up limit about one hundred percent. Beyond the theoretical model, a more direct way to understand would be the band structure. Figure 3 give the band structure of bulk Mn_2Au and CdO, the density of states (DOS) and Fermi surface of Mn_2Au . At the $\text{Mn}_2\text{Au}/\text{CdO}$ interface with O bonded with Mn (we can deduce the formation of Mn-O bond from the Mn-O distance around 1.93 \AA), the former would change the DOS of the latter. Compared with the DOS of Mn atom in the bulk Mn_2Au , the DOS peaks of the \uparrow spin of the d states of the interfacial Mn atom is downward shift, while that of the \downarrow spin upward shift and shrink greatly. The change lead to enhanced spin polarization of the interfacial Mn atoms at the Fermi energy. The orbit dependent DOS of interfacial Mn atom shown in the inset of Fig. 3C indicates that the p and d orbits contribute mainly to the \uparrow spin, and the total DOS of the \uparrow spin is about four fold larger than that of the \downarrow spin. According to Julliere's model[38], the MR should be around 250%, which is close to the calculated value in the AF-MTJs with S1 structure with thinner CdO barrier but considerable smaller than that with thicker barriers.

For the $k_{||}$ resolved barrier nature of tetragonal Mn_2Au , the barrier thickness of Nb/ Mn_2Au (24)/CdO(10)/ Mn_2Au (24)/Nb AF-MTJ is $k_{||}$ dependent also. It is about 2.4 and 9.1 nm for the $k_{||}$ points within and out of the Sharvin area of Mn_2Au , respectively. From the band structure (Fig. 3A), we can find that $k_{||}$ points within or close to the Sharvin area of Mn_2Au can satisfy the resonance condition, which maybe responsible

for the giant TMRs found in the AF-MTJs with thicker CdO barrier.

Complex band structure can be used to estimate the tunnel transmission through the barrier. Figure 4 gives the complex band structure of bulk CdO and Mn_2Au at 2D Γ point and a resonant $k_{||}$ point along the [001] direction. Here, we pay attention to the complex band with smaller imaginary part in the vicinity of Fermi energy. The symmetry of the imaginary bands can be identified by the symmetry of the connected real bands. Rocksalt CdO has crystal structure as MgO, and the complex band structure of CdO is similar to that of MgO. In Fig. 4A, we can identify a Δ_1 imaginary band connecting with a s band (band r3 of Fig. 4A) and a d_{z^2} band (band r1 of Fig. 4A) at Γ point, and a Δ_5 imaginary band connecting with a doubly degenerate bands d_{zx} and d_{zy} (band r2 of Fig. 4A). Between the Δ_1 and Δ_5 imaginary bands, the symmetry of the imaginary band i2 is hard to identify. The Δ_1 imaginary band shows smaller κ ($k = k_z + i\kappa$) in the vicinity of the Fermi energy, which would dominate the tunneling transmission, indicating the potential symmetry filtering application as found in the Fe/MgO/Fe junction[21]. Furthermore, semiconductor type band gap and small effective mass at Γ point (Fig. 3B) is another favorable character for the spintronic application.

The symmetry of the imaginary bands of tetragonal Mn_2Au is complex. There presents two parabolic imaginary bands with evident Δ_1 symmetry and several irregular imaginary bands at the 2D Γ point. The Δ_1 imaginary band i3 is connected with band r2 and r4 at Z point, and another Δ_1 imaginary band (with larger κ) connected with band r1 and r3 at Γ point, as shown in Fig. 4C. To identify the symmetry of the irregular band, especially the one (band i1) with smallest κ , we studied the Fermi surface (FS) around and beyond the Fermi energy as shown in Fig 3D. Therein, the symmetry of both FS A and B are energy dependent. At energy $E_F - 0.3 \text{ eV}$, the FS B shows four fragments sited around $\phi = 0, 90, 180$ and 270 degrees with d_{xy} (or $d_{x^2-y^2}$) symmetry, which form an onion rings structure around $E_F - 0.5\text{eV}$, and then turn into thin square drum with small gaps at four corners around $E_F - 1.0\text{eV}$, and then the square drum gets thicker and the gaps expands until two sheets sited parallel to the xy face formed around $E_F - 1.7\text{eV}$. Within energy range from $E_F - 1.0\text{eV}$ to $E_F - 1.7\text{eV}$, The FS B can be identified as a combination of p_z and d_{z^2} symmetry. For the imaginary band i1 is connected with a d_{xy} orbit, which can be identified as a Δ_2 symmetry.

At Fermi energy, the electron is predicted to decay with the rate $\exp(-2\kappa\Delta_z)$, where Δ_z is the thickness of barrier. According to the symmetry filtering scheme,[21] bands can and only can accommodate incoming states with same symmetry as itself. Firstly, we pay attention to the Δ_1 symmetry states. Along the transport direction, we can estimate that κa_z is about 0.37π for the Δ_1 electrons of CdO, and 1.62π for the Δ_1 electrons of Mn_2Au . Supposing a symmetric AF-MTJ with 24Ls Mn_2Au and

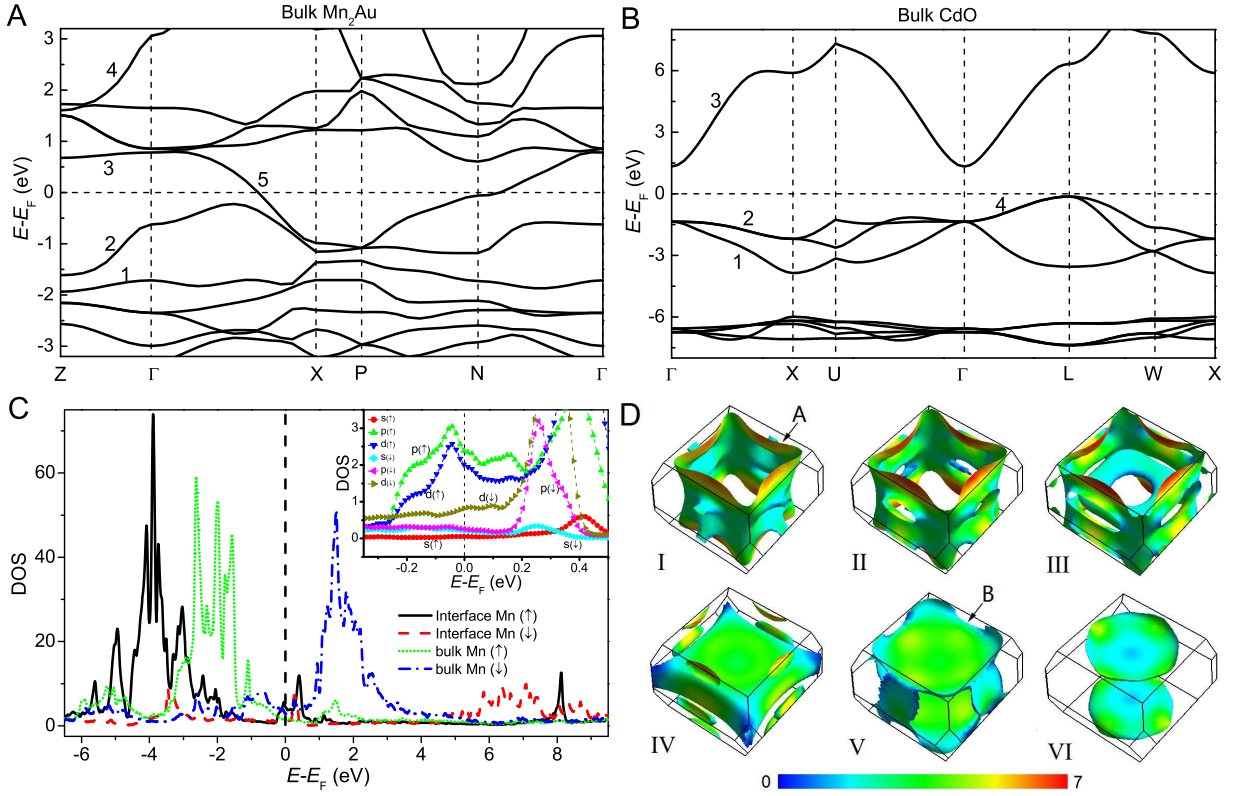


FIG. 3: (A) Band structure of rocksalt CdO and (B) tetragonal Mn₂Au calculated using mBJ potential. (C) Density of states (DOS) of the bulk and interfacial Mn atoms with positive magnetic moment of the ideal Mn₂Au/CdO(10)/Mn₂Au multilayer. Inset of (C): orbit dependent DOS of the interfacial Mn atom. In (A), band with index 1, 2, 3 and 4 are flat bands from the Γ (0 0 0) to Z (0.5 0.5 -0.5), and 5 from Γ to X (0 0 0.5). In (B), band with index 1, 2 and 3 are bands from the Γ to X (0.5 0 0.5) point, and 4 from Γ to L (0.5 0.5 0.5). (D) Fermi surfaces FSs of tetragonal bulk Mn₂Au around Fermi energy E_F , $E_F - 0.3$ eV, $E_F - 0.5$ eV, $E_F - 1.0$ eV, $E_F - 1.5$ eV, and $E_F - 1.7$ eV. The color bar is the Fermi velocity with Rydberg atomic unit. There shows two FSs range from E_F to $E_F - 1.7$. The FS A present at E_F and disappearing around $E_F - 1.0$ eV is band 5 shown in (A), and the FS B appearing around $E_F - 0.3$ eV and disappearing around $E_F - 1.7$ eV is band 2 shown in (B).

10Ls CdO, the tunneling transmission of the Δ_1 states at the 2D Γ point would be about 4.1×10^{-41} e²/h. Supposing the imaginary band i2 of CdO follows same symmetry as the imaginary band i1 of Mn₂Au, the former has κa_z of 1.11π and the latter 0.67π . The spin transmission in the AF-MTJs carried by the Δ_2 state would be around 1.7×10^{-30} e²/h. Comparatively, the transmission in the ideal Nb/Mn₂Au(24)/CdO(10)/Mn₂Au(24)/Nb AF-MTJs with S1 structure calculated based on the scattering wave function is about 1.0×10^{-49} and 3.7×10^{-51} e²/h for the P and AP magnetic states, respectively. Our calculations indicate that the Δ_1 imaginary band should be responsible for the spin transmission the 2D Γ points. Many effects should be responsible for the giant difference between the model and the first-principles calculations. The leading factors should be band mismatch, the interface scattering, the electron mass entering into the barriers, and so on.

For $k_{||}$ points slightly away the 2D Γ points, the average spin transmission calculated first-principally of the $k_{||}$ points within $|k_x| \leq \pi/100$ and $|k_y| \leq \pi/100$ is about 1.2×10^{-29} and 2.3×10^{-33} e²/h for the P and AP

magnetic states of the ideal Nb/Mn₂Au(24)/CdO(10)/Mn₂Au(24)/Nb AF-MTJs with S1 structure, respectively. The calculated numbers are about twenty orders in magnitude larger than that calculated at the 2D Γ point, which is about ten orders in magnitude larger than the model estimation carried by the Δ_1 states, but close to the model estimation carried by the Δ_2 states (supposing the imaginary band i2 of CdO follows a Δ_2 symmetry).

As the $k_{||}$ points walk outward from the 2D Γ point, the $k_{||}$ dependent barrier height and band gap of rock-salt CdO would decrease for the join of the band from Γ to X (band 4 in Fig. 3B). Similar effect is found in tetragonal Mn₂Au, also. When the interfaces in the AF-MTJs are clean enough, some $k_{||}$ points with appropriate barrier height maybe meet the resonant tunneling condition. For the ideal "Nb lead" AF-MTJs, the barrier is so thick that only the $k_{||}$ points within or close to the Sharvin area of Mn₂Au can meet the resonant tunneling conditions. For a resonant $k_{||}$ points within the Sharvin area of Mn₂Au with $k_x a_0 = 0.161$ and $k_y a_0 = 1.60$ as shown in Fig. 4B and D, the imaginary part of the wave

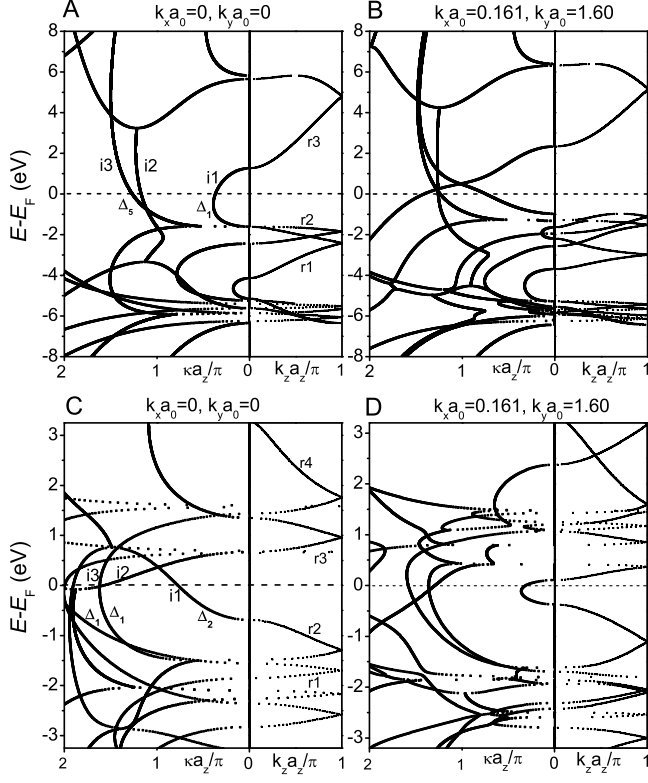


FIG. 4: Complex band structure of the sandwiched (a-b) CdO and (c-d) Mn₂Au in the Mn₂Au/CdO/Mn₂Au AF-MTJs at 2D Γ and one resonance $k_{||}$ points. Therein, k_z and κ are real and imaginary part of wave vector k , $a_0 = 3.328$ nm is the lateral lattice parameter of the scattering region, and a_z is the thickness of the repeat unit along the transport direction, which is 4.69 and 8.539 nm for CdO and Mn₂Au, respectively. The real part bands are folding. Bands with index r1, r2, and r3 in (a) are corresponding to the bands with index 1, 2, and 3 in Fig. 4(c), respectively, and Bands with index r1, r2, r3 and r4 in (c) are corresponding to the bands with index 1, 2, 3, and 4 in Fig. 4(b), respectively.

vector contribute by the d states are considerable smaller than that at the 2D Γ point as shown in Fig. 4A and C, respectively. That is, the interfacial resonant tunneling is directly responsible for the giant TMRs effect in the pure AF-MTJs with thicker CdO, but the $k_{||}$ dependent band structure of the system is more fundamental.

C. Voltage bias dependence of TMRs

Another effect of the complex band structures in the "Nb lead" AF-MTJs would be the voltage bias dependent TMR effect as shown in Fig. 5. When voltage bias is finite, the potentials in the CdO region shift linearly while that in the Mn₂Au region keep unchange for the metallicity, which would affect the interfacial resonance.[36] So, the spin transmissions in the ideal Nb/Mn₂Au(24)/CdO(10)/Mn₂Au(24)/Nb AF-MTJs would be sensitive

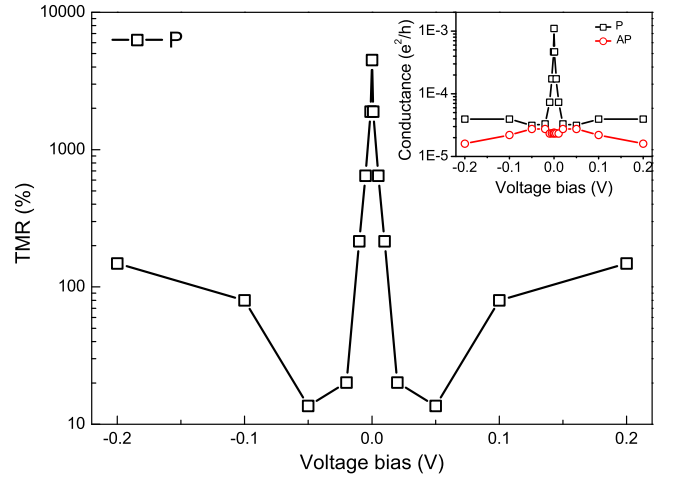


FIG. 5: Voltage bias dependent TMRs and conductances in the ideal Nb/Mn₂Au(24)/CdO(10)/Mn₂Au(24)/Nb pure AF-MTJs with S1 structure.

to the voltage bias. A voltage bias of 0.001eV can reduce the spin transmission in the P magnetic state of the AF-MTJs with S1 structure by a factor of twenty as shown in the inset of Fig. 5. Comparatively, the total spin transmission of the AP magnetic state of the AF-MTJs is not so sensitive to the voltage bias. As a result, the TMR of the AF-MTJs junction decrease firstly from 4500% at equilibrium state to 14% at voltage bias of 0.05 eV, and then turn to increase to 150% at 0.2 eV.

Table I summarizes the conductances and TMRs of the ideal Nb/Mn₂Au(24)/CdO(10)/Mn₂Au(24)/Nb(001) AF-MTJs at zero and 0.1 eV voltage bias. At equilibrium state, the symmetric structures show larger tunneling conductances and TMRs than the asymmetric ones, and the S1 structure shows largest tunneling conductance among all studied cases, and the S3 structure shows largest TMRs among all studied cases. In the presence of voltage bias of 0.1 eV, the tunneling conductances of the P and PP magnetic states of the symmetric structures S1 and S3 are more sensitive to the voltage bias, while the AP structure of which are insensitive to the voltage bias, leading to sharp decrease of the TMR effect. The S2 structure is an exception among the symmetric structures, both the tunnel conductances and TMRs are insensitive to the finite voltage bias. The P, PP and AP magnetic states of the asymmetric structures A1 and A2 show similar effect in the presence of voltage bias, the TMRs in the two structure is insensitive to the voltage bias also. The A3 structure is an exception among the asymmetric structures, both the tunneling conductances and TMRs increase under finite voltage bias. Summarily, the tunneling conductance and TMR effect in the ideal "Nb lead" AF-MTJs show complex dependence on the magnetic structures, the atomic structures, and the voltage bias. These complex dependence can be understood by the complex band structure of the CdO and Mn₂Au in companion with

TABLE I: Tunneling conductances and TMRs of the ideal Nb/Mn₂Au(24)/CdO(10)/Mn₂Au(24)/Nb(001) pure AF-MTJs at zero and 0.1 eV (in the bracket) voltage bias. The unit of conductance is $10^{-5} e^2/h$.

Structures	P	AP	PP	TMR(P) (%)	TMR(PP) (%)
S1	110(3.96)	2.35(2.20)	77.2(3.16)	4580(80)	3180(44)
S2	4.28(1.36)	0.180(0.101)	2.27(0.737)	2270(1250)	1160(536)
S3	0.925(0.0667)	0.011(0.0191)	0.49(0.0429)	8300(250)	4350(125)
A1	0.468(0.0369)	0.279(0.0230)	0.375(0.0301)	68(60)	34(31)
A2	0.0583(0.0250)	0.0348(0.0136)	0.0466(0.0199)	67(84)	34(46)
A3	0.967(1.55)	0.68(0.755)	0.773(1.19)	42(105)	14(57)
S1 ¹	9.15	2.59	-	252	-
S1 ²	28.9	12.9	-	123	-
S1 ³	10.4	2.61	-	298	-

¹ 10% Oxygen vacancies at both Mn₂Au/CdO interfaces

² 10% Manganese vacancies at both Mn₂Au/CdO interfaces

³ 10% Manganese-Cadmium (Mn-Cd) exchanges at both Mn₂Au/CdO interfaces

the localized magnetism at the Mn₂Au/CdO interface induced by interfacial effect as discussed above.

D. Interfacial disorder

Ideal heterostructure is hard to realize experimentally, many kinds imperfections present and concentrate at the interfaces. Here, we pay attention to three kinds imperfections as shown in the Table I. Generally, the introductions of interfacial disorder would deteriorate the interfacial resonance tunneling effect between the same spin channels while enhance the scattering probability among the different spin channels.[36] Compared with interfacial Oxygen vacancy and Manganese-Cadmium (Mn-Cd) exchanges with same concentration, the interfacial Manganese vacancy enhance the scattering probability among the different spin channels more. The presence of 10% interfacial imperfections would reduce the TMRs in the Nb/Mn₂Au(24)/CdO(10)/Mn₂Au(24)/Nb(001) AF-MTJs to around one or several hundreds percent at equilibrium state. To achieve larger TMR effect in the AF-MTJs, the interfaces should be as clean as possible.

order of 1000% are found in some symmetric junctions while that around 100% found in some asymmetric junctions. The interfacial resonance tunneling effect related with the $k_{||}$ dependent band structures of the system and enhanced magnetism of the interfaces atoms should be responsible for the giant TMR effect therein. The TMR effect in the ideal AF-MTJs is sensitive to the interfacial structure, voltage bias, and interfacial disorder. For a ideal symmetric junction with S1 structure with 24 Ls Mn₂Au and 10 Ls CdO, a voltage bias of 0.1 eV would reduce the TMR from 4580% at equilibrium state to 80%, and the introduction of 10% interfacial disorder such as O vacancy, Mn vacancy, and Mn-Cd exchanges at the Mn₂Au/CdO interfaces would reduce the TMR to the order of one to several hundreds percent at the equilibrium state. The giant TMR effect predicted in the pure AF-MTJs indicates the possibility to exploit the anti-ferromagnetism without the aid of ferromagnet or ferri-magnet. Moreover, good symmetry filtering effect in companion with the semiconductor-type band gap suggests rocksalt CdO a promising material for spintronic applications.

IV. SUMMARY

Summarily, we calculate the spin transmission and TMR effect in the Mn₂Au-based pure AF-MTJs based on a first-principle scattering theory. Giant TMRs with

Acknowledgement

We gratefully acknowledge financial support from the National Natural Science Foundation of China (Grant No. 12074102, 11804062 and 11804310).

-
- [1] T. Jungwirth, X. Marti, P. Wadley, and J. Wunderlich, Nat. Nanotech. **11**, 231 (2016).
 - [2] V. Baltz, A. Manchon, M. Tsoi, T. Moriyama, T. Ono, and Y. Tserkovnyak, Rev. Mod. Phys. **90**, 015005 (2018).
 - [3] A. S. Núñez, R. A. Duine, P. Haney, and A. H. MacDonald, Phys. Rev. B **73**, 214426 (2006).
 - [4] X.-T. Jia, X.-L. Cai, and Y. Jia, Sci. China-Phys. Mech.

- Astron. **63**, 297512 (2020).
- [5] X. Jia, H. Tang, S. Wang, and M. Qin, Phys. Rev. B **95**, 064402 (2017).
- [6] Y. Zhu, X. Y. Guo, L. N. Jiang, Z. R. Yan, Y. Yan, and X. F. Han, Phys. Rev. B **103**, 134437 (2021).
- [7] Z. Yan, R. Zhang, X. Dong, S. Qi, and X. Xu, Phys. Chem. Chem. Phys. **22**, 14773 (2020).

- [8] X. Guo, B. Yang, X. Zhang, Y. Zhu, X. Han, and Y. Yan, Phys. Rev. B **104**, 144423 (2021).
- [9] J. Yang, S. Fang, Y. Peng, S. Liu, B. Wu, R. Quhe, S. Ding, C. Yang, J. Ma, B. Shi, et al., Phys. Rev. Appl. **16**, 024011 (2021).
- [10] B. Wu, J. Yang, R. Quhe, S. Liu, C. Yang, Q. Li, J. Ma, Y. Peng, S. Fang, J. Shi, et al., Phys. Rev. Appl. **17**, 034030 (2022).
- [11] H. Yang, Q. Liu, Z. Liao, L. Si, P. Jiang, X. Liu, Y. Guo, J. Yin, M. Wang, Z. Sheng, et al., Phys. Rev. B **104**, 214419 (2021).
- [12] J. Dong, X. Li, G. Gurung, M. Zhu, P. Zhang, F. Zheng, E. Y. Tsymlal, and J. Zhang, Phys. Rev. Lett. **128**, 197201 (2022).
- [13] L. Šmejkal, A. B. Hellenes, R. González-Hernández, J. Sinova, and T. Jungwirth, Phys. Rev. X **12**, 011028 (2022).
- [14] C. Song, Y. You, X. Chen, X. Zhou, Y. Wang, and F. Pan, Nanotechnology **29**, 112001 (2018).
- [15] E. V. Gomonay and V. M. Loktev, Low Temp. Phys. **40**, 17 (2014).
- [16] P. Wadley, B. Howells, J. Železný, C. Andrews, V. Hills, R. P. Campion, V. Novák, K. Olejník, F. Maccherozzi, S. S. Dhesi, et al., Science **351**, 587 (2016).
- [17] S. Y. Bodnar, L. Šmejkal, I. Turek, T. Jungwirth, O. Gomonay, J. Sinova, A. Sapozhnik, H.-J. Elmers, M. Kläui, and M. Jourdan, Nat. Commun. **9**, 348 (2018).
- [18] N. Bhattacharjee, A. A. Sapozhnik, S. Y. Bodnar, V. Y. Grigorev, S. Y. Agustsson, J. Cao, D. Dominko, M. Obergfell, O. Gomonay, J. Sinova, et al., Phys. Rev. Lett. **120**, 237201 (2018).
- [19] X. F. Zhou, J. Zhang, F. Li, X. Z. Chen, G. Y. Shi, Y. Z. Tan, Y. D. Gu, M. S. Saleem, H. Q. Wu, F. Pan, et al., Phys. Rev. Appl. **9**, 054028 (2018).
- [20] Y. Deng, X. Liu, Y. Chen, Z. Du, N. Jiang, C. Shen, E. Zhang, H. Zheng, H.-Z. Lu, and K. Wang, National Science Review p. nwac154 (2022).
- [21] W. H. Butler, X.-G. Zhang, T. C. Schulthess, and J. M. MacLaren, Phys. Rev. B **63**, 054416 (2001).
- [22] J. Mathon and A. Umerski, Phys. Rev. B **63**, 220403 (2001).
- [23] S. Ikeda, K. Miura, H. Yamamoto, K. Mizunuma, H. Gan, M. Endo, S. Kanai, J. Hayakawa, F. Matsukura, and H. Ohno, Nat. Mater. **9**, 721 (2010).
- [24] X.-T. Jia, X.-L. Cai, W.-Y. Yu, L.-W. Zhang, B.-J. Wang, G.-H. Cao, S.-Z. Wang, H.-M. Tang, and Y. Jia, J. Phys. D: Appl. Phys. **53**, 245001 (2020).
- [25] X. Zhou, X. Chen, J. Zhang, F. Li, G. Shi, Y. Sun, M. Saleem, Y. You, F. Pan, and C. Song, Phys. Rev. Appl. **11**, 054030 (2019).
- [26] P. N. Hai, J. Magn. Soc. Jpn **44**, 137 (2020).
- [27] V. Barthém, C. Colin, H. Mayaffre, M.-H. Julien, and D. Givord, Nat. Commun. **4**, 2892 (2013).
- [28] G. Kresse and J. Furthmüller, Phys. Rev. B **54**, 11169 (1996).
- [29] I. Turek, V. Drchal, J. Kudrnovský, M. Sob, and P. Weinberger, *Electronic Structure of Disordered Alloys, Surfaces and Interfaces* (Kluwer, Boston, 1997).
- [30] F. Tran and P. Blaha, Phys. Rev. Lett. **102**, 226401 (2009).
- [31] X. Liu, C. Li, S. Han, J. Han, and C. Zhou, Appl. Phys. Lett. **82**, 1950 (2003).
- [32] R. Chandiramouli and B. Jeyaparakash, Solid State Sci. **16**, 102 (2013).
- [33] S. Wang, Y. Xu, and K. Xia, Phys. Rev. B **77**, 184430 (2008).
- [34] Y. Ke, K. Xia, and H. Guo, Phys. Rev. Lett. **100**, 166805 (2008).
- [35] A. B. Shick, S. Khmelevskiy, O. N. Mryasov, J. Wunderlich, and T. Jungwirth, Phys. Rev. B **81**, 212409 (2010).
- [36] Y. Ke, K. Xia, and H. Guo, Phys. Rev. Lett. **105**, 236801 (2010).
- [37] X. Jia, K. Xia, and G. E. W. Bauer, Phys. Rev. Lett. **107**, 176603 (2011).
- [38] M. Julliere, Phys. Lett. A **54**, 225 (1975).